Mechanism and Machine Theory

Volume 92, October 2015, Pages 184–199

Time-Dependent Reliability Analysis for Function Generation Mechanisms with Random Joint Clearances

Junfu Zhang
School of Mechanical Engineering
Xihua University
Chengdu, Sichuan 610039, P.R.China

Xiaoping Du[1]
Department of Mechanical and Aerospace Engineering
Missouri University of Science and Technology
Rolla, Missouri 65409, U.S.A.

Abstract

Time-dependent reliability method for mechanisms predicts the probability of satisfying the motion requirement in a predefined period of time. The current reliability methods do not consider the random clearances in mechanism joints. This work extends the current methods into function generation mechanisms on which the effect of random joint clearances is significant. The motion output is approximated in the first order with respect to random dimension variables and in a higher order with respect to random joint clearances by the Hybrid Dimension Reduction Method. This treatment achieves an optimal balance between accuracy and efficiency. Then an envelope method is used to calculate the time-dependent reliability. The method is demonstrated by the analysis of three four-bar function generation mechanisms.

Keywords: Time-dependent reliability, function generator, joint clearance.

[1] Corresponding author: 400 West 13th Street, Toomey Hall 272, Rolla, MO 65409, U.S.A. Tel: 1-573-341-7249, E-mail: dux@mst.edu

Nomenclature

C	Revolute joint
e	Distance between centers of a bearing and a journal
g	Motion error function
L	Vector of random dimension variables
L	A component of L
m	Size of L
$p_f(\mu)$	Point probability of failure at θ
$p_f(\mu_0;\mu_f)$	Interval probability of failure on $[\mu_0;\mu_f]$
p	Number of expansion points
q	Number of random clearance variables
$R(\mu)$	Point reliability at θ
$R(\mu_0;\mu_f)$	Interval reliability on $[\mu_0;\mu_f]$
r	Rank of covariance matrix §
r_c	Radius of the clearance circle
S	Random variables
X	Vector of the x-coordinates of random clearance variables
X	Component of X
Y	Vector of the y-coordinates of random clearance variables
Y	Component of Y
¨	Allowable motion error
µ	Input angle
μ_g	Mean of the motion error
μ_L	Mean of the dimension variable L
μ_z	Vector of the means of the motion error at expansion points
§	Covariance matrix of the motion errors at expansion points
σ_g	Standard deviation of the motion error
σ_L	Standard deviation of the dimension variable L
©	Cumulative distribution function of a standard normal distribution
Ã	Actual motion output
$\tilde{A}_d$	Desired motion output

1. INTRODUCTION

Appropriate joint clearances are chosen for ensuring mechanisms work properly. On the other hand, they may be somewhat uncontrollable due to manufacturing imprecision and wearing [1]. They are in fact stochastic [2], and the uncertainty in clearances can be propagated to the motion output, thereby affecting adversely the

kinematic and dynamic performances of mechanisms [1-5]. The effects might be the motion accuracy loss, unreliability, and reduced service life. They become more severe on high-speed and micro-mechanical systems, such as those in aerospace applications, intelligent robots, and numerically controlled machine tools.

Studies on joint clearances include the investigations on their effects on mechanisms performance and dynamic characteristics [6]. For the latter, the effects of revolute joint clearances on dynamic characteristics are modeled with three major strategies – the massless link approach, the spring-damper approach, and the momentum exchange approach [7]. Among the three approaches, the third approach is more realistic and is widely employed to study the mechanism dynamic with joint clearances. For examples, Erkaya [8] presented a modeling and optimization approach to reduce the undesired effects of joint clearances on a walking mechanism. Another study of Erkaya [9] established a contact model in a revolute joint with clearance by using the nonlinear spring-damper characteristic and then investigated the kinematic and dynamic characteristics of the welding robot manipulator with joint clearance. Flores et al. [10-13] investigated the effects of joint clearances on kinematics and dynamics of planar and spatial mechanisms with rigid and elastic links. Another study of Flores [14] proposed a general and comprehensive approach to automatically adjust the time step with variable time-step integration algorithms, in the vicinity of contact of multi-body systems. Varedi et al.[15] proposed an optimization method to alleviate the undesirable effect of joint clearance. Zhang et al. [16] established a simulation model of joint clearance with the Hertzian normal contact force model and a Coulomb-type friction force model, and then established a polynomial function Kriging meta-model for optimizing the performance of

a mechanical system with the revolute joint clearance. Zhang et al. [17] established the dynamic equations for a 3-RRR parallel mechanism by using Newton-Euler equations with Lankarani-Nikravesh contact force model and improved Coulomb friction force model, and then investigated the dynamic performances of the 3-dof mechanism with multi-clearance joints.

For kinematic characteristics, the focus is the quantification of the effect of joint clearances on the ability of achieving desired positions or orientations precisely [6]. There are two types of methods in this area. The first type includes deterministic methods, and they are used to specify the mechanism motion error resulted from joint clearances without considering the randomness in the joint clearances. In the deterministic approaches, many researchers used a massless virtual link to model the joint clearance and investigated the motion accuracy for the planar mechanisms [1, 18, 19]. In the error analysis of the spatial mechanisms and manipulators, the virtual work method [6, 20], the screw theory method [21-23], and the interval method [24] have been proposed to study the effects of joint clearance on position and orientation deviation of the manipulators. Based on the theory of envelope, Chen [25] presented a geometric method to uniformly construct the indeterminate influences of the input uncertainties and the joint clearance on the pose (position and orientation) deviation of the manipulators. The other type contains probabilistic methods [2, 26-31], which rely on probability and statistics for creating stochastic models of joint clearances and the uncertainty propagation. In general, the probability density function (PDF) is used to describe the random behavior of a joint clearance variable in a clearance circle [2]. The uniform distribution and normal distribution are commonly used for the probabilistic model of the joint clearance [2, 26].

Although the stochastic approach does not explore the contact kinematic models of the pairing elements of a joint, it is more desirable for important applications where reliability is of great interest.

A reliability method is the major method among the probabilistic methods. The mechanism reliability is the probability of the output member's position and/or orientation falling within a specified range from the desired position and/or orientation [32]. Higher kinematic reliability means a higher chance to achieve the required motion. It is the reason that reliability methods have been extensively applied in mechanism analysis and synthesis [26-39].

There are two types of kinematic reliability, including point kinematic reliability and time-dependent (interval) kinematic reliability [38]. The former reliability is defined at a specific instance of time and can provide instantaneous information at a specific point in the motion interval of a mechanism. Most of the methods in the literature of mechanism reliability analysis and synthesis are for point kinematic reliability, which is usually calculated by the First Order Second Moment (FOSM) method and Monte Carlo Simulation (MCS) [26, 28, 30-36].

Recently, the methods for the time-dependent (interval) kinematic reliability have also been proposed [38]. This kind of reliability is defined in a period of time (a time interval), which indicates the range of the motion input where the desired motion output is defined. The first passage method with the Poisson approximation [38] has been recently used, and the envelope method [39] has also been proposed to estimate the interval kinematic reliability. The former method is based on the upcrossing probability, which is the probability that the motion error exceeds the failure threshold at a time instant. The

method assumes that all the upcrossings during the period of time under consideration are independent. If multiple dependent upcrossings occur, the calculated probability of failure will be much larger than the true value. The envelope method improves the accuracy by using an envelope that covers all the extreme values of the motion error during the period of time. The envelope function is at first identified by FOSM and is approximated at a limited number of time instants where the possible extreme values of the motion error might occur. Then the probability of failure is estimated at these time instants through an integration with respect to a multivariate normal distribution.

None of the above methods handles random joint clearances. The current reliability methods that can deal with random joint clearances are for only point reliability. The commonly used FOSM and the First Order Reliability Method (FORM) are inaccurate [26] when random joint clearances are involved. The reason is that the coordinates of a pin center are confined within its clearance circle and are therefore statistically dependent. As a result, the first order approximation of the motion output with respect to the clearance variables will lose the dependency and produce poor accuracy. For a good balance between the accuracy and efficiency, the Hybrid Dimension Reduction Method (HDRM) [26] is proposed. It employs the first order approximation for independent dimension variables and bivariate (or trivariate) dimension reduction for dependent joint clearance variables. HDRM can produce more accurate solutions than FOSM or FORM while maintaining higher efficiency than MCS.

To fill the gap in dealing with joint clearances for interval kinematic reliability, this work develops a new reliability method for such an analysis. The new method combines the envelope method (originally for interval reliability without clearances) and HDRM

(originally for point reliability with clearances) and extend the integrated method to interval reliability analysis with clearances.

In Section 2, we review the kinematic analysis of four-bar planar function generation mechanisms and then discuss the probabilistic model for joint clearances using HDRM. In Section 3, we discuss how to combine HDRM with the envelope method to calculate the interval kinematic reliability. Three numerical examples are presented in Section 4 followed by conclusions in Section 5.

2. MOTION ERROR MODELING

In this section, we use the planar four-bar linkage to show how to establish the probabilistic model of the motion error with joint clearances by HDRM.

2.1.Kinematic analysis

A planar four-bar linkage with joint clearances is shown in Fig.1. The crank *AB* is the input member with the input angle μ, and the rocker *CD* is the output member with the output angle Ã.

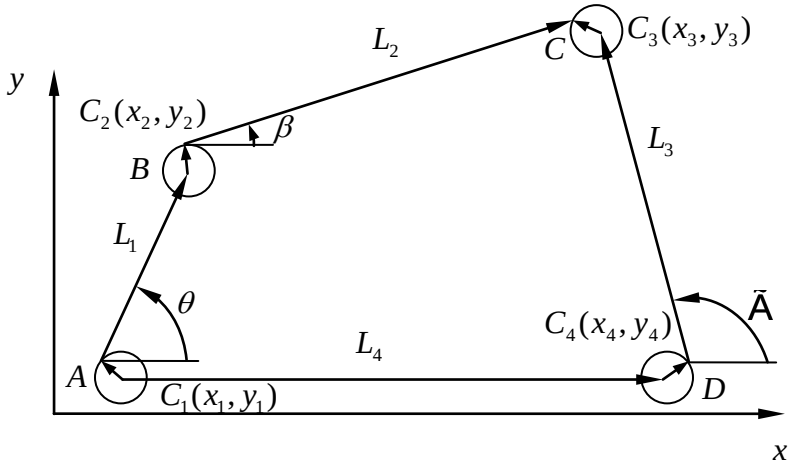

Figure 1 Four-bar mechanism with joint clearances

The dimension variables are the lengths $L = (L_1; L_2; L_3; L_4)^T$. They are assumed to be statistically independent. As commonly reported in the mechanism literature, the elements of L follow normal distributions, $L_i \sim N(\mu_{Li}; \sigma_{Li}^2)$ $(i = 1; \ldots; m)$, where μ_{Li} and σ_{Li} are the mean and the standard deviations of L_i, respectively; σ_{Li} can be determined by the tolerance of L_i with the 3-sigma rule. For the linkage in Fig. 1, $m = 4$.

C_1, C_2, C_3 and C_4 are the four revolute joints. The existence of clearances in these joints is inevitable due to machining tolerances, wear, material deformation, and imperfections. A general joint between links i and j is shown in Fig. 2. The clearance circle [2, 26] is the circle with a radius of $r_c = r_B - r_J$, where r_B and r_J are radii of the bearing and journal, respectively. Let the distance between the center of a bearing and the origin be e_j; namely

$$e_j = \sqrt{X_j^2 + Y_j^2} \tag{1}$$

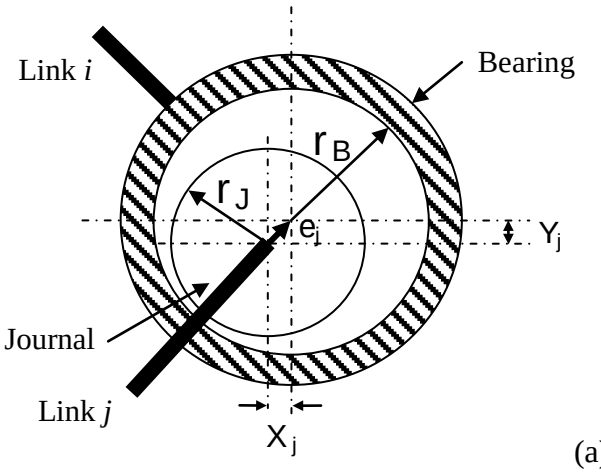

(a)

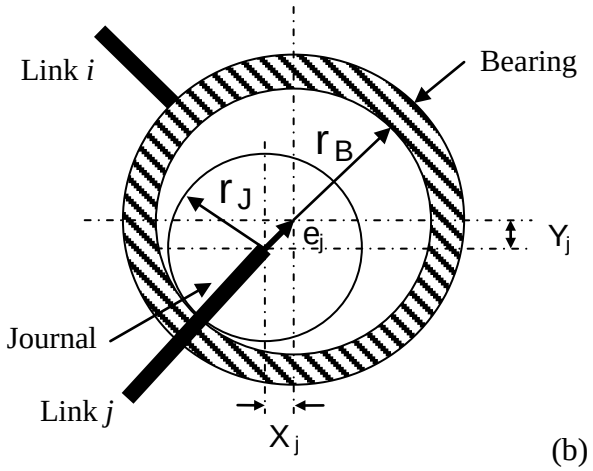

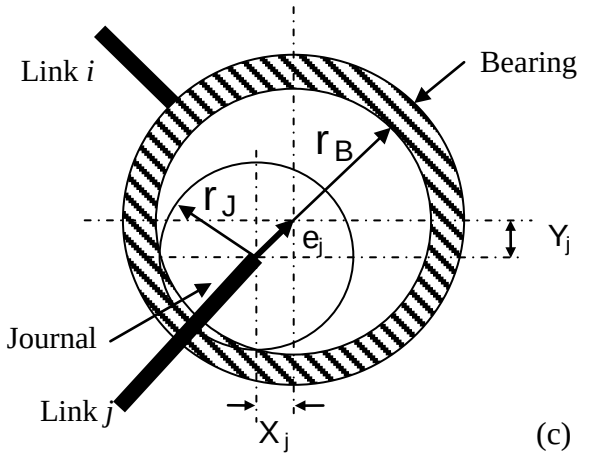

Figure 2 Joint clearance

Three types of motion between the journal and bearing are defined in [8, 9] as

$$\pm_j = \begin{cases} e_j \ge r_{Cj} & \text{free-flight mode} \\ e_j = r_{Cj} & \text{contact with impact mode} \\ e_j > r_{Cj} & \text{continuous contact mode (relative penetration)} \end{cases} \tag{2}$$

The three types are shown as Cases (a), (b), and (c), respectively, in Fig. 2.

In case of small clearances, the free-flight mode and impact mode dominate [9]. For large clearances, all the three types of motion are possible. Large clearances are relatively rare for function generation mechanisms. To this end, we consider only small

clearances and therefore assume that the center of a bearing varies randomly within the associated clearance circle. For planar mechanisms, the coordinates of the bearing centers are $(X;Y) = ((X_1;Y_1);::::;(X_q;Y_q))^T$. For the four-bar linkage in Fig.1, $q = 4$. X_j and Y_j are statistically dependent because they are confined within their clearance circle C_j $(j = 1;::::;q)$.

The center of the journal varies randomly inside the clearance circle. In literature, the joint PDF of the coordinates X_j and Y_j of the center is assumed either uniform or normal [2, 26]. Herein we use the more conservative uniform distribution, and the results can be easily extended to the normal distribution or any other distributions. With this assumption, X_j and X_j follow a uniform distribution defined within the clearance circle of radius r_{cj} as follows [2, 26]:

$$f_{X_j;Y_j}(x;y) = \begin{cases} \frac{1}{\pi r_{cj}^2} & \text{if } x^2 + y^2 \cdot r_{cj}^2 \\ 0 & \text{otherwise} \end{cases} \tag{3}$$

The loop-closure equations of crank-rocker mechanism are given by (see Fig. 1)

$$\begin{cases} L_1\cos\mu + L_2\cos\bar{} - L_3\cos\tilde{A} + X_1 + X_2 - X_3 - X_4 = 0 \\ L_1\sin\mu + L_2\sin\bar{} - L_3\sin\tilde{A} + Y_1 + Y_2 - Y_3 - Y_4 = 0 \end{cases} \tag{4}$$

Eliminating $\bar{}$, we obtain the motion output $\tilde{A}$ as

$$\tilde{A} = 2\arctan\left(\frac{-B \pm \sqrt{A^2 + B^2 - C^2}}{C - A}\right) \tag{5}$$

where $A = 2EL_3$, $B = 2FL_3$, $C = E^2 + F^2 + L_3^2 - L_2^2$,

$E = -L_1\cos\mu + L_4 + X_1 + X_2 - X_3 - X_4$

$F = L_1\sin\mu - Y_1 - Y_2 + Y_3 + Y_4$

2.2. Motion error

A function generation mechanism is designed so that the relative motion between links connected to the ground satisfies a functional relationship $y = f(x)$. Let x be defined on interval $[x_0; x_e]$, the initial angle of crank be μ_0, the range of motion input be $[\mu_0; \mu_e]$, the corresponding initial angle of rocker be $\tilde{A}_0$, and the range of motion output be $[\tilde{A}_0; \tilde{A}_e]$. Then the desired motion output $\tilde{A}_d$ at μ is given by

$$\tilde{A}_d(\mu) = \tilde{A}_0 + \frac{\Delta \tilde{A}}{\Delta f} \left[\frac{\Delta x}{\Delta \mu}(\mu - \mu_0) - f(x_0) \right] \tag{6}$$

where $\Delta f = f(x_e) - f(x_0)$, $\Delta x = x_e - x_0$, $\Delta \mu = \mu_e - \mu_0$, and $\Delta \tilde{A} = \tilde{A}_e - \tilde{A}_0$.

The motion error is the difference between the actual motion output $\tilde{A}$ and the desired motion output $\tilde{A}_d$ and is given by

$$g(S; \mu) = \tilde{A}(S; \mu) - \tilde{A}_d(\mu) \tag{7}$$

where $S = (L; (X; Y))$.

In Eq. (7), the random variables $S = (L; (X; Y))$ are time independent. $g(S; \mu)$ varies, however, with respect to the input angle μ. In other words, the motion error $g(S; \mu)$ is a function of the time factor μ and is therefore a stochastic process. Its statistical moment functions are also time dependent because the actual motion output $\tilde{A}(S; \mu)$ and the desired motion output $\tilde{A}_d(\mu)$ are generally nonlinear functions of μ. As a result, $g(S; \mu)$ is in general a non-stationary stochastic process. The nonstationality makes the reliability analysis difficult. Other challenges also exist [26]. For example, the dependence between clearance variables X and Y, the nonlinearity of $g(S; \mu)$ with respect to random variables, and high dimensionality of random variables for a

mechanism with a large number of members. Next, we use HDRM to simplify the motion error and then derive the probabilistic model of the motion error.

2.3. Probabilistic motion error model

We use HDRM [26] to build a probabilistic model of the motion error. HDRM is originally proposed to analyze the point kinematic reliability of mechanisms with joint clearances [26]. It can effectively and accurately handle the statistically dependent clearance variables. As shown in what follows, it can also be extended to interval kinematic reliability analysis. We at first briefly review HDRM and then use it to derive the moment and standard deviation functions of the motion error with respect to time.

Since the dimension variables are independent, the motion error can be approximated by the sum of univariate functions of dimension variables. Since the *x*- and *y*-coordinates of clearances are strongly dependent, the motion error is approximated by the sum of bivariate functions of the *x*-*y* clearance coordinates [26]. Adding the time factor μ to the original equation in [26], we have the approximation given by

$$\begin{aligned} g(S;\mu) = g(L;(X;Y);\mu) \approx \\ g_0 + \sum_{i=1}^{m} g_{L_i}(L_i;\mu) \\ + \sum_{j=1}^{q} \left[g_{X_j}(X_j;\mu) + g_{Y_j}(Y_j;\mu) + g_{X_jY_j}((X_j;Y_j);\mu) \right] \end{aligned} \tag{8}$$

The terms on the right-hand side of Eq. (8) are explained below.

$$g_0 = g(\mu_S;\mu) = g(\mu_L;(\mu_X;\mu_Y);\mu) \tag{9}$$

where $\mu_L = (\mu_{L_1};\cdots;\mu_{L_m})$, $\mu_X = (\mu_{X_1};\cdots;\mu_{X_q})$, and $\mu_Y = (\mu_{Y_1};\cdots;\mu_{Y_q})$.

$$g_{L_i}(L_i;;\mu) = g((L_i;\mu_S^{\gg L_i});\mu) - g_0 \tag{10}$$

where $(L_i;\mu_S^{\gg L_i}) = (\mu_{L_1};\cdots;\mu_{L_{i-1}};L_i;\mu_{L_{i+1}};\cdots;\mu_{L_m};(\mu_X;\mu_Y))$.

$$g_{X_j}(X_j;\mu) = g((X_j;{}^1_S{}^{\gg X_j});\mu) - g_0 \tag{11}$$

where $(X_j;{}^1_S{}^{\gg X_j}) = ({}^1_L;({}^1_{X_1};\cdots;{}^1_{X_{j-1}};X_j;{}^1_{X_{j+1}};\cdots;{}^1_{X_m};{}^1_Y))$.

$$g_{Y_j}(Y_j;\mu) = g((Y_j;{}^1_S{}^{\gg Y_j});\mu) - g_0 \tag{12}$$

where $(Y_j;{}^1_S{}^{\gg Y_j}) = ({}^1_L;({}^1_X;{}^1_{Y_1};\cdots;{}^1_{Y_{j-1}};Y_j;{}^1_{Y_{j+1}};\cdots;{}^1_{Y_m}))$.

$$g_{X_jY_j}((X_j;Y_j);\mu) = g((X_j;Y_j;{}^1_S{}^{\gg X_jY_j});\mu) - g_{X_j}(X_j;\mu) - g_{Y_j}(Y_j;\mu) - g_0 \tag{13}$$

where
$(X_j;Y_j;{}^1_S{}^{\gg X_jY_j}) = ({}^1_L;({}^1_{X_1};\cdots;{}^1_{X_{j-1}};X_j;{}^1_{X_{j+1}};\cdots;{}^1_{X_m};{}^1_{Y_1};\cdots;{}^1_{Y_{j-1}};Y_j;{}^1_{Y_{j+1}};\cdots;{}^1_{Y_m}))$.

Simplifying Eq. (8), we have

$$\begin{aligned} g(S;\mu) \approx \hat{g}(L;(X;Y);\mu) = & \sum_{i=1}^{m} g((L_i;{}^1_S{}^{\gg L_i});\mu) \\ & + \sum_{j=1}^{q} g((X_j;Y_j;{}^1_S{}^{\gg X_jY_j});\mu) - (m+q-1)g({}^1_S;\mu) \end{aligned} \tag{14}$$

The first order Taylor series expansion is accurate with respect to dimension variables L because the standard deviations of L are small. We can then simplify the univariate functions $g((L_i;{}^1_S{}^{\gg L_i});\mu)$ $(i=1,\cdots,m)$ by replacing $g((L_i;{}^1_S{}^{\gg L_i});\mu) - g({}^1_S;\mu)$ with $\frac{\partial g(S;\mu)}{\partial L_i}\Big|_{{}^1_S}(L_i - {}^1_{L_i})$. Hence, $\hat{g}(L;(X;Y);\mu)$ becomes

$$\begin{aligned} \hat{g}(L;(X;Y);\mu) = & \sum_{i=1}^{m} \frac{\partial g(S;\mu)}{\partial L_i}\Big|_{{}^1_S}(L_i - {}^1_{L_i}) + \sum_{j=1}^{q} g((X_j;Y_j;{}^1_S{}^{\gg X_jY_j});\mu) \\ & - (q-1)g({}^1_S;\mu) \end{aligned} \tag{15}$$

Let $R_j = g((X_j;Y_j;{}^1_S{}^{\gg X_jY_j});\mu)$. R_j is assumed to be approximately normally distributed, namely, $R_j \gg N({}^1_{R_j};\sigma^2_{R_j})$. We then transform all random variables into those that follow standard normal distributions and rewrite Eq. (15) as

$$\hat{g}(L;(X;Y)) = a_0 + \sum_{i=1}^{m} a_i\sigma_{L_i}U_i + \sum_{j=1}^{q}\sigma_{c_j}U_j \tag{16}$$

where $a_0 = \sum_{j=1}^{q} {}^{1}r_{c_j} - (q-1)g({}^{1}S;\mu)$ and $a_i = \frac{\partial g(S;\mu)}{\partial L_i}\Big|_{{}^{1}S}$. Both a_0 and a_i are functions of the time factor μ. U_i and U_j follow standard normal distributions $U_i \sim N(0;1^2)$ $(i = 1;\ldots;m)$ and $U_j \sim N(0;1^2)$ $(j = 1;\ldots;q)$. ${}^{1}r_{c_j}$ and σ_{c_j} are the mean and standard deviation of R_j, respectively, and ${}^{1}r_{c_j}$ and σ_{c_j} are calculated by the Gaussian cubature method [40]. Using the 7-point rule given in [41], ${}^{1}r_{c_j}$ is evaluated by

$$ {}^{1}r_{c_j} = E\left\{ g((X_j;Y_j;{}^{1}_{S}\vec{X}_j\vec{Y}_j);\mu)\right\} = \sum_{i=1}^{7} w_i\, g((x_j;y_j;{}^{1}_{S}\vec{x}_j\vec{y}_j);\mu) \tag{17} $$

and σ_{c_j} is evaluated by

$$ \sigma^2_{c_j} = D\left\{ g((X_j;Y_j;{}^{1}_{S}\vec{X}_j\vec{Y}_j);\mu)\right\} = \sum_{i=1}^{7} w_i\, g((x_j;y_j;{}^{1}_{S}\vec{x}_j\vec{y}_j);\mu) - {}^{1}r^2_{c_j} \tag{18} $$

where $(x_1;y_1) = (0;0)$, $(x_i;y_i) = (\pm r\sqrt{2/3};0)$, for $i = 2;3$, and $(x_i;y_i) = (\pm r\sqrt{1/6};\pm r\sqrt{1/2})$ for $i = 4$ through 7 with $w_1 = \frac{1}{4}$ and $w_i = \frac{1}{8}$ for $i = 1$ through 2.

Recall that $S = (L;(X;Y))$. From Eq. (16), the mean ${}^{1}g(S;\mu)$ of $g(S;\mu)$ is computed by

$$ {}^{1}g(S;\mu) = a_0 \tag{19} $$

and the variance $\sigma^2_g(S;\mu)$ of $g(S;\mu)$ is

$$ \sigma^2_g(S;\mu) = \sum_{i=1}^{m} a_i^2\sigma^2_{L_i} + \sum_{j=1}^{q} \sigma^2_{c_j} \tag{20} $$

We have obtained the mean and standard deviation functions of the motion error stochastic process. Since the motion error at any given instant of time is normally distributed, the motion error stochastic process is in general a non-stationary Gaussian process. To fully describe the Gaussian process, we also need to know its auto-correlation

function, which captures the dependence of the motion errors at any two time instances. We will discuss how to obtain the auto-correlation function in the next section when we present the envelope method.

3. KINEMATIC RELIABILITY ANALYSIS

In this section, we discuss the new interval reliability method with joint clearances. We also briefly review the point reliability because we also use it in the evaluation of the interval reliability.

3.1. Point kinematic reliability

The point reliability is defined at a specific instance of time. For a function generation mechanism, the point kinematic reliability at μ is the probability that the motion error $g(S;\mu)$ is less than the allowable motion error ε. The motion of the mechanism is considered satisfactory if the motion error is small enough such that

$$|g(S;\mu)| = |\tilde{A}(S;\mu) - \tilde{A}_d(\mu)| \le \varepsilon \tag{21}$$

Then the point reliability $R(\mu)$ at μ is defined by the following probability

$$R(\mu) = \Pr\{|g(S;\mu)| \le \varepsilon\} = \Pr\{-\varepsilon \le g(S;\mu) \le \varepsilon\} \tag{22}$$

where $\Pr\{\cdot\}$ stands for a probability.

The point probability of failure is then given by

$$p_f(\mu) = \Pr\{|g(S;\mu)| > \varepsilon\} = \Pr\{g(S;\mu) > \varepsilon \cup g(S;\mu) < -\varepsilon\} \tag{23}$$

The mechanism is in a working condition if $|g(S;\mu)| \le \varepsilon$ and is in a failure condition otherwise. Then $R(\mu)$ represents the likelihood that the mechanism works properly at μ regardless whether it has failed or not before that.

FOSM calculates the point reliability by

$$R(\mu) = \Phi\left(\frac{\varepsilon - \mu_{g}(S;\mu)}{\sigma_{g}(S;\mu)}\right) - \Phi\left(\frac{-\varepsilon - \mu_{g}(S;\mu)}{\sigma_{g}(S;\mu)}\right) \tag{24}$$

and the point probability of failure defined in Eq. (23) is then given by

$$p_f(\mu) = 1 - \Phi\left(\frac{\varepsilon - \mu_{g}(S;\mu)}{\sigma_{g}(S;\mu)}\right) + \Phi\left(\frac{-\varepsilon - \mu_{g}(S;\mu)}{\sigma_{g}(S;\mu)}\right) \tag{25}$$

where $\Phi(\phi)$ is the cumulative distribution function (CDF) of a standard normal variable.

3.2. Interval kinematic reliability

Time-dependent (interval) kinematic reliability is defined over a time interval and can provide complete reliability information over the entire motion range of interest. The time interval is the range of the motion input where the desired function is defined. Interval reliability is the probability that the motion error is always less than the specified allowance ε over an interval of motion input $[\mu_0; \mu_e]$ and is defined by [38]

$$\begin{aligned} R(\mu_0;\mu_e) &= Pr\{|g(S;\mu)| \le \varepsilon;\ \forall \mu \in [\mu_0;\mu_e]\} \\ &= Pr\{-\varepsilon \le g(S;\mu) \le \varepsilon;\ \forall \mu \in [\mu_0;\mu_e]\} \end{aligned} \tag{26}$$

where $\forall$ is a universal quantifier, meaning “for all”. The corresponding interval probability of failure is given by

$$\begin{aligned} p_f(\mu_0;\mu_e) &= Pr\{|g(S;\mu)| > \varepsilon;\ \exists \mu \in [\mu_0;\mu_e]\} \\ &= Pr\{g(S;\mu) > \varepsilon \cup g(S;\mu) < -\varepsilon;\ \exists \mu \in [\mu_0;\mu_e]\} \end{aligned} \tag{27}$$

where $\exists$ is a existential quantifier, meaning “there exists”.

As indicated in Eqs. (19) and (20), both $\mu_g(S;\mu)$ and $\sigma_g(S;\mu)$ are dependent on μ and are hence time dependent. $g(S;\mu)$ is therefore a non-stationary Gaussian process. The mean value first-passage (MVFP) method [38] has been used to solve for the interval kinematic reliability. This method is based on FOSM and the first-passage method with the Poisson approximation [38]. Since the Poisson approximation neglects the statistical dependence between the events of upcrossing the failure threshold, MVFP may not be

accurate for some problems. For improving the accuracy of the time-dependent mechanism reliability analysis, an envelope approach [39] has been proposed. But it is only for problems without joint clearances. In the next two subsections, we discuss our new development that extends the envelope method into problems where joint clearances are accommodated.

3.3. Envelope method with joint clearances

An envelope function of the motion error $g(S;\mu)$ on $[\mu_0;\mu_e]$ [39] is a function of S and encloses all the motion errors on $[\mu_0;\mu_e]$. Once $[\mu_0;\mu_e]$ is given, the envelope function is time independent. Denote the envelope functions by $G^+(S) = 0$ and $G^i(S) = 0$ for failure boundaries $g(S;\mu) = "$ and $g(S;\mu) = ¡ "$, respectively.

$G^+(S)$ is determined by [39]

$$\begin{cases} g(S;\mu) = " \\ g_{\mu}(S;\mu) = 0 \end{cases} \tag{28}$$

and $G^i(X)$ is given by

$$\begin{cases} g(S;\mu) = ¡ " \\ g_{\mu}(S;\mu) = 0 \end{cases} \tag{29}$$

Next, we explain how to use the envelope functions to estimate the interval reliability. As shown in Fig. 3, at the limit state, $g(S;\mu) = "$ represents a family of hyper-surfaces of $g(S;²) = "$, where μ changes within $[\mu_0;\mu_e]$. $G^+(S)$ is a hyper-surface that is tangent to each member of the family of hyper-surfaces of $g(S;²) = "$. In the other case, some members of hyper-surfaces of $g(S;²) = "$ may not touch with $G^+(S) = 0$. In both cases, $G^+(S)$ is the worst-case failure-safety boundary for limit state ". For the same reason, $G^i(S)$ is the worst-case failure-safety boundary for limit state ¡ ".

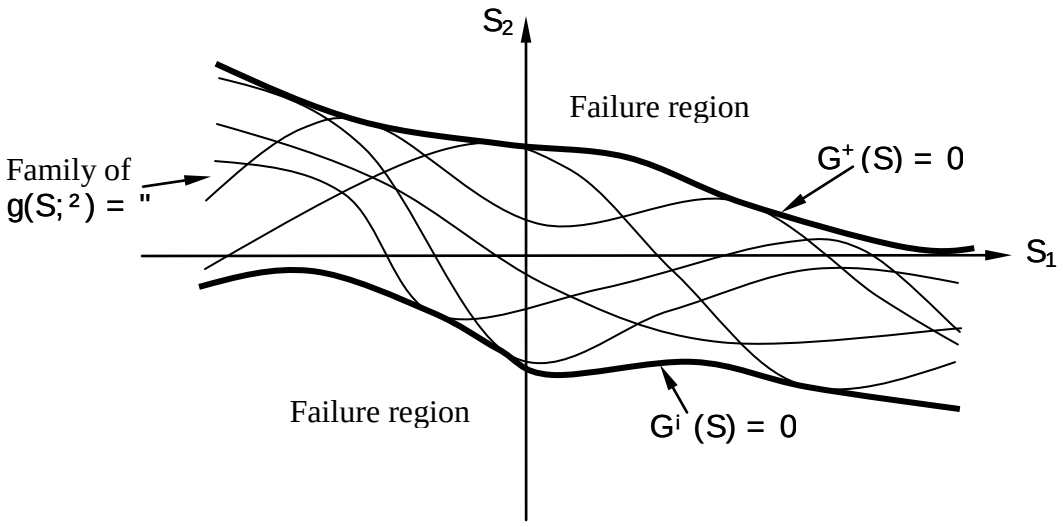

Figure 3 Envelope functions of the motion error

The time-dependent reliability analysis requires the use of the worst-case motion errors. The interval reliability defined in Eq. (26) is equivalent to

$$R(\mu_0;\mu_e) = \Pr\left\{ \max_{\mu} g(S;\mu) \ 6 \ " \ \backslash \ \min_{\mu} g(S;\mu) > \ ¡ \ "; \ 8\mu \ 2 \ [\mu_0;\mu_e] \right\} \tag{30}$$

where $\max_{\mu} g(S;\mu)$ and $\min_{\mu} g(S;\mu)$ are the global maximum and minimum values of the motion error on $[\mu_0;\mu_e]$. Both of the extreme values are only functions of random variables S. This indicates that the interval reliability requires the extreme values of the motion error which are represented by $G^+(S)$ and $G^i(S)$.

For the above reason, the interval reliability can be calculated by

$$R(\mu_0;\mu_f) = \Pr\left\{ G^+(S) < 0 \backslash \ G^i(S) > 0 \right\} \tag{31}$$

The analysis is now converted to a time-independent problem. The equations for $G^+(S)$ and $G^i(S)$ have been derived in [39] and are also given in the Appendix.

The two envelope functions are nonlinear functions and can be approximated at a number of expansion points. The reason of using multiple expansion points is to deal with the high nonlinearity of the extreme motion error (worst-case motion error).

Selecting proper expansion points is critical for the accuracy of the reliability analysis. Theoretically, the probability of failure is the integral of the joint PDF of random variables over the failure region of the worst-case motion error. It is natural to select expansion points that have highest joint probability densities or highest values of the integrand because they have highest contribution to the integral. After expansion points μ_i ($i = 1; 2; ¢¢¢; p$) are identified, the probability of failure becomes the probability of a union of events that are associated the motion errors at μ_i. Since the motion errors at μ_i are normally distributed and are correlated, the reliability can therefore be estimated by integrating the joint PDF of the motion errors at μ_i. The integral is given by

$$R(\mu_0; \mu_i) = \int_0^{\infty} \frac{1}{(2\pi)^{r=2} |\Sigma|^{1=2}} \exp\left[-\frac{1}{2}(Z - \mu_z)\Sigma^{-1}(Z - \mu_z)^T \right] dZ \qquad (32)$$

in which

$$\mu_z = (\mu_{g1}; \mu_{g2}; ¢¢¢; \mu_{gp}) \qquad (33)$$

and

$$\Sigma = \begin{bmatrix} D_{11} & D_{12} & ¢¢¢ & D_{1p} \\ & D_{22} & ¢¢¢ & D_{2p} \\ & & \ddots & \vdots \\ & & & D_{pp} \end{bmatrix} \qquad (34)$$

μ_{gi} ($i = 1; 2; ¢¢¢; p$) is the mean of the motion error at the expansion point μ_i and is given in Eq. (19); D_{ij} is the covariance between $g(S; \mu_i)$ and $g(S; \mu_j)$, where $i; j = 1; 2; ¢¢¢; p$. D_{ij} is given by

$$D_{ij} = \begin{cases} \psi_g(S; \mu_i) & \text{if } i = j \\ b(\mu_S; \mu_i) ¢ b(\mu_S; \mu_j) & \text{if } i \neq j \end{cases} \qquad (35)$$

where the dot means an inner product, $\psi_g(S; \mu_i)$ is given in Eq. (20), and $b(\mu_S; \mu_i)$ is given in Eq. (37).

The covariance matrix Σ should be a positive-definite matrix. If the requirement is not met, some of the time instants are redundant and should be eliminated. If the rank of Σ is r, then we eliminate $p - r$ time instants, where the point probabilities of failure over $[t_0, t_e]$ are smallest. Suppose after the elimination, the time instants are t_i^c, $i = 1, 2, \cdots, r$. The corresponding mean vector and covariance matrix are denoted by μ_z^0 and Σ^c, respectively. We then replace μ_z and Σ with μ_z^0 and Σ^c, respectively, and then apply Eq. (32) to calculate the interval reliability.

3.4. Numerical procedure

The procedure of computing the interval kinematic reliability is summarized in Fig.4. The steps in the procedure are explained below.

Step 1. Set initial parameters, such as the means and standard deviations of the dimension variables, the clearance radii, the allowable error limit, and the ranges of the motion input and motion output.

Step 2. Perform the deterministic mechanism analysis to obtain the structural error $g(\mu_S; \mu)$ and the coefficient $\frac{\partial g(S;\mu)}{\partial L_i}\Big|_{\mu_S}$.

Step 3. Calculate $a_0 = \sum_{j=1}^{q} \mu_{rc_j} - (q-1) g(\mu_S; \mu)$, $a_i = \frac{\partial g(S;\mu)}{\partial L_i}\Big|_{\mu_S}$, μ_{rc_j}, and σ_{rc_j} using Eqs. (17) and (18), and then calculate the mean $\mu_g(S;\mu)$ and variance $\sigma_g^2(S;\mu)$ of $g(S;\mu)$ by Eq. (19) and (20), respectively. In this step, the deterministic mechanism kinematic analysis is called.

Step 4. Calculate the point kinematic reliability $R(\mu)$ using Eq. (24) or the point probability $p_f(\mu)$ of failure using Eq. (25).

Step 5. Solve for μ_i^+ for $G^+(U) = 0$ and μ_i^j for $G^j(U) = 0$ using Eqs. (41) and (41), respectively. This step calls the deterministic mechanism kinematic analysis to obtain $b_0(\cdot_S;\mu)$, $b_0^0(\cdot_S;\mu)$, $b(\cdot_S;\mu)$ and $b^0(\cdot_S;\mu)$.

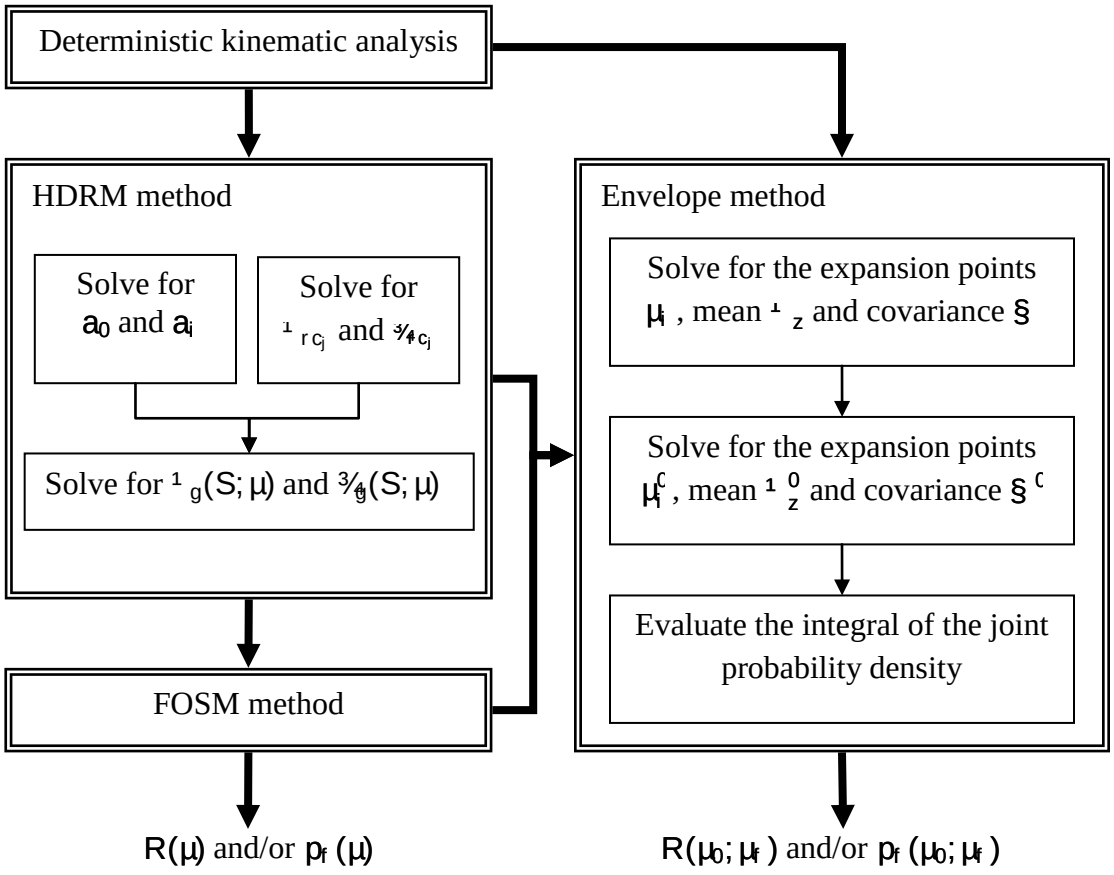

Figure 4 Procedure of kinematic reliability analysis with clearances

Step 6. Using the expansion points μ_i (those are the solutions from Step 5), calculate the mean $\cdot_{gi}$ $(i = 1;2;\cdots;p)$ by Eq. (19) and the covariance D_{ij} by Eq. (35), and then construct the mean vector $\cdot_z$ and covariance matrix $\S$ with Eqs. (43) and (44).

Step 7. Calculate the rank r of Σ. If the rank r is less than p, and eliminate $p - r$ time instants where the point probabilities of failure are the least. Then construct a new covariance matrix Σ^c and a mean vector μ_z^0.

Step 8. Calculate the interval reliability with Eq. (32). In this step, a numerical integration method is applied to calculate the multivariate normal CDF.

4. NUMERICAL EXAMPLES

In this section, we use a four-bar linkage mechanism with three required functions as examples to demonstrate the proposed method.

4.1. Sine function generation mechanism

The desired function is defined by $y = \sin x$ with $x = [x_0; x_e] = [0^\circ; 90^\circ]$. The initial angle of the crank is $\mu_0 = 95.1^\circ$, and the range of the input angle is $\Delta\mu = 120^\circ$. The initial angle of the rocker is $\tilde{A}_0 = 90.6^\circ$, and the range of the output angle is $\Delta\tilde{A} = 60^\circ$. The distributions of the dimension variables are given in Table 1. As discussed in Sec. 2.1, the coordinates of the journal centers are assumed to follow uniform distributions defined within the clearance radii r_{c_j} $(j = 1; 2; 3; 4)$, and the associated distributions are shown in Table 2.

A failure occurs when the absolute error of the motion output is greater than $\varepsilon = 0.27^\circ$, or when $|g(S)| > 0.27^\circ$.

Table 1. Random dimensions of the sine mechanism

Variable	Mean (mm)	Standard deviation (mm)	Distribution
L_1	$\mu_{L_1} = 52.2$	$\sigma_{L_1} = 0.03$	Normal
L_2	$\mu_{L_2} = 104.9$	$\sigma_{L_2} = 0.03$	Normal
L_3	$\mu_{L_3} = 67.6$	$\sigma_{L_3} = 0.03$	Normal
L_4	$\mu_{L_4} = 100$	$\sigma_{L_4} = 0.03$	Normal

Table 2. Random clearances of the sine mechanism

Variable	Clearance radius r_c (mm)	Distribution
$(X_1; Y_1)$	0.02	2D-uniform within a circle
$(X_2; Y_2)$	0.02	2D-uniform within a circle
$(X_3; Y_3)$	0.02	2D-uniform within a circle
$(X_4; Y_4)$	0.02	2D-uniform within a circle

We used the proposed method to solve for the kinematic reliability of this mechanism. The results are given in Table 3 and are plotted in Fig. 5, where $\phi\mu = \mu - \mu_0$. We also used the Monte Carlo Simulation (MCS) solution as a benchmark for the accuracy comparison. The sample size of MCS is 10^6, and the 95% confidence interval of the MCS solution is also provided in Table 3. The results indicate that the solutions of the new method are very close to those of MCS and are therefore accurate. The error with respect to the MCS solution is defined by

$$\text{error}\% = \frac{p_f - MCS_{solution}}{MCS_{solution}} \times 100\% \tag{36}$$

The numbers of function calls (deterministic mechanism analyses) and the computational time by the proposed method are also listed in Tables 3, which indicates that the proposed method is much more efficient than MCS. A regular personal computer was used for the reliability analysis.

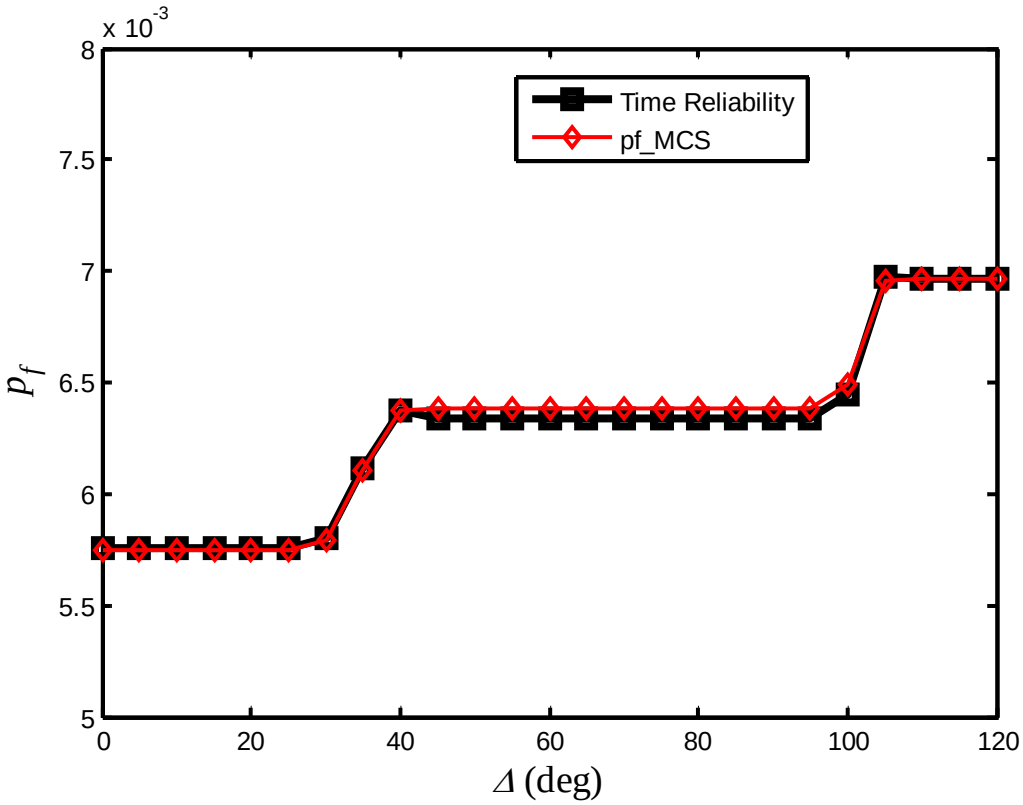

Figure 5 $p_f(\mu_0;\mu_e)$ of the sine mechanism

Table 3. $p_f(\mu_0;\mu_e)$ of the sine mechanism

$[\mu_0;\mu_e](^{\pm})$	Proposed method	MCS	95% MCS confidence interval	error (%)	Number of function evaluations	Computational time (seconds)	
						Proposed method	MCS
[95.1,95.1]	5.75×10^{-3}	5.75×10^{-3}	$[5.60, 5.90]\times10^{-3}$	0.06	114	0.09	1.57
[95.1,105.1]	5.75×10^{-3}	5.75×10^{-3}	$[5.60, 5.90]\times10^{-3}$	0.06	234	0.08	189
[95.1,115.1]	5.75×10^{-3}	5.75×10^{-3}	$[5.60, 5.90]\times10^{-3}$	0.06	232	0.06	185
[95.1,125.1]	5.81×10^{-3}	5.79×10^{-3}	$[5.65, 5.94]\times10^{-3}$	0.19	232	0.07	187
[95.1,135.1]	6.38×10^{-3}	6.38×10^{-3}	$[6.22, 6.53]\times10^{-3}$	0.01	350	0.13	184
[95.1,145.1]	6.34×10^{-3}	6.38×10^{-3}	$[6.23, 6.54]\times10^{-3}$	0.67	350	0.11	186
[95.1,155.1]	6.34×10^{-3}	6.38×10^{-3}	$[6.23, 6.54]\times10^{-3}$	0.63	350	0.12	189
[95.1,165.1]	6.34×10^{-3}	6.38×10^{-3}	$[6.23, 6.54]\times10^{-3}$	0.63	350	0.12	177
[95.1,175.1]	6.34×10^{-3}	6.38×10^{-3}	$[6.23, 6.54]\times10^{-3}$	0.66	466	0.14	182
[95.1,185.1]	6.34×10^{-3}	6.38×10^{-3}	$[6.23, 6.54]\times10^{-3}$	0.65	466	0.15	188
[95.1,195.1]	6.45×10^{-3}	6.49×10^{-3}	$[6.33, 6.64]\times10^{-3}$	0.58	466	0.14	184
[95.1,205.1]	6.97×10^{-3}	6.97×10^{-3}	$[6.80, 7.13]\times10^{-3}$	0.04	582	0.16	187
[95.1,215.1]	6.97×10^{-3}	6.97×10^{-3}	$[6.80, 7.13]\times10^{-3}$	0.07	582	0.17	186

4.2. Inverse tangent function generation mechanism

The desired function is defined by $y = \arctan x$ with $t \in [x_0; x_e] = [0; 1]$. The initial angle of the crank is $\mu_0 = 104{:}37^{\pm}$, and the range of the input angle is $\Delta\mu = 100^{\pm}$. The initial angle of the rocker is $\tilde{A}_0 = 92{:}68^{\pm}$, and the range of the output angle is $\Delta\tilde{A} = 45^{\pm}$. The distributions of the dimension variables are given in Table 4. The centers of the joints are assumed uniform within the clearance radii r_{c_j} ($j = 1; 2; 3; 4$), and the associated distributions are shown in Table 6, where $\Delta\mu = \mu_i - \mu_0$. The failure is defined by the event when the absolute error of the output motion is greater than $\varepsilon = 0{:}20^{\pm}$, or by the event where $|g(S; \mu)| > 0{:}20^{\pm}$.

The results for the inverse tangent function generator are given in Table 6 and are plotted in Fig. 6. The sample size of MCS is 10^6, and the 95% confidence interval of the MCS solution is also provided in Table 6. The results show that proposed method is accurate with respect to the MCS solution. The error of the proposed method is smaller than 2% for time intervals from $\mu \in [104{:}37^{\pm}; 104{:}37^{\pm}]$ to $\mu \in [104{:}37^{\pm}; 204{:}37^{\pm}]$ (or time intervals from $\Delta\mu \in [0^{\pm}; 0^{\pm}]$ to $\Delta\mu \in [0^{\pm}; 100^{\pm}]$), except the longest time interval $\mu \in [104{:}37^{\pm}; 204{:}37^{\pm}]$, which responds to the interval of $\Delta\mu \in [0^{\pm}; 100^{\pm}]$.

Table 4. Random dimensions of the inverse tangent mechanism

Variable	Mean (mm)	Standard deviation (mm)	Distribution
L_1	$^1_{L_1} = 57{:}95$	$\sigma_{L_1} = 0{:}035$	Normal
L_2	$^1_{L_2} = 121{:}47$	$\sigma_{L_2} = 0{:}035$	Normal
L_3	$^1_{L_3} = 109{:}78$	$\sigma_{L_3} = 0{:}035$	Normal
L_4	$^1_{L_4} = 100$	$\sigma_{L_4} = 0{:}035$	Normal

Table 5. Random clearances of inverse the tangent mechanism

Variable	Clearance radius r_c (mm)	Distribution
$(X_1; Y_1)$	0.015	2D-uniform within a circle
$(X_2; Y_2)$	0.015	2D-uniform within a circle
$(X_3; Y_3)$	0.015	2D-uniform within a circle
$(X_4; Y_4)$	0.015	2D-uniform within a circle

Table 6. $p_f(\mu_0; \mu_e)$ of the inverse tangent mechanism

$[\mu_0; \mu_e]$ $(^{\pm})$	Proposed method	MCS	95% MCS confidence interval	error (%)	Number of function evaluations	Computational time (seconds)	
						Proposed method	MCS
[104.37, 104.37]	6.65×10^{-4}	6.66×10^{-4}	$[6.15, 7.17]\times10^{-4}$	0.21	114	0.21	1.57
[104.37, 114.37]	6.65×10^{-4}	6.66×10^{-4}	$[6.15, 7.17]\times10^{-4}$	0.21	234	0.09	187
[104.37, 124.37]	6.71×10^{-4}	6.71×10^{-4}	$[6.20, 7.22]\times10^{-4}$	0.00	234	0.06	191
[104.37, 134.37]	3.72×10^{-3}	3.70×10^{-3}	$[3.58, 3.82]\times10^{-3}$	0.45	234	0.06	188
[104.37, 144.37]	4.95×10^{-3}	4.99×10^{-3}	$[4.85, 5.13]\times10^{-3}$	0.84	350	0.17	192
[104.37, 154.37]	4.95×10^{-3}	4.99×10^{-3}	$[4.85, 5.13]\times10^{-3}$	0.83	350	0.15	189
[104.37, 164.37]	4.95×10^{-3}	4.99×10^{-3}	$[4.85, 5.13]\times10^{-3}$	0.83	350	0.11	197
[104.37, 174.37]	4.98×10^{-3}	5.02×10^{-3}	$[4.88, 5.16]\times10^{-3}$	0.83	350	0.11	202
[104.37, 184.37]	7.20×10^{-3}	7.28×10^{-3}	$[7.12, 7.45]\times10^{-3}$	1.15	466	0.20	209
[104.37, 194.37]	7.18×10^{-3}	7.28×10^{-3}	$[7.11,7.44]\times10^{-3}$	1.29	466	0.13	200
[104.37, 204.37]	7.89×10^{-3}	8.41×10^{-3}	$[8.23, 8.59]\times10^{-3}$	6.22	466	0.13	200

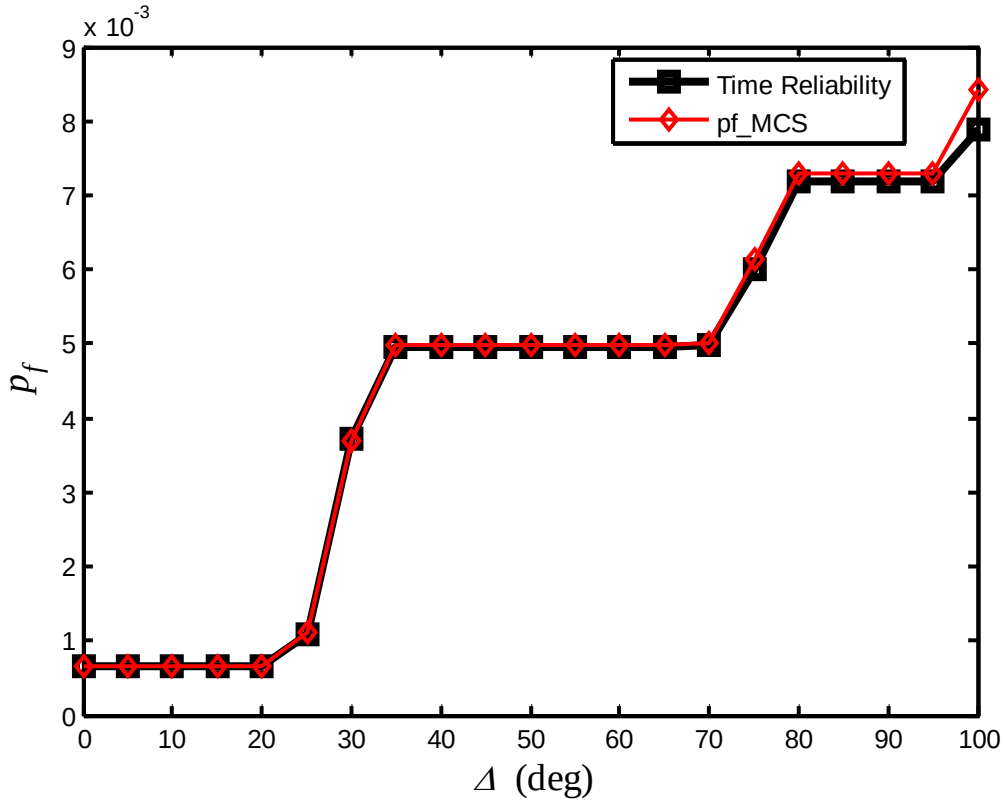

Figure 6 $p_f(\mu_0;\mu_e)$ of the inverse tangent mechanism

4.3. Combined trigonometric function generation mechanism

To further test the proposed method, we now combine the two trigonometric functions (cosine and tangent functions) for the desired function, which is defined by $y = \cos(x) + 0{:}6\tan(x{=}3)$ with $x \in [x_0; x_e] = [45^{\pm}; 120^{\pm}]$. The initial angle of the crank is $\mu_0 = 55{:}68^{\pm}$, and the range of the input angle is $\Delta\mu = 100^{\pm}$. The initial angle of the rocker is $\tilde{A}_0 = 76^{\pm}$, and the range of the output angle is $\Delta\tilde{A} = 60^{\pm}$. The distributions of the dimension variables are given in Table 7. The centers of the joints are assumed uniform within the clearance radii r_{c_j} $(j = 1; 2; 3; 4)$, and the associated distributions are shown in Table 8, where $\Delta\mu = \mu_i - \mu_0$. The failure is defined by the event when the

absolute error of the output motion is greater than $\varepsilon = 0.31^{\circ}$, or by the event where $|g(S;\mu)| > 0.31^{\circ}$.

Table 7. Random dimensions of the combined trigonometric function mechanism

Variable	Mean (mm)	Standard deviation (mm)	Distribution
L_1	$\mu_{L_1} = 56.28$	$\sigma_{L_1} = 0.03$	Normal
L_2	$\mu_{L_2} = 96.44$	$\sigma_{L_2} = 0.03$	Normal
L_3	$\mu_{L_3} = 85.71$	$\sigma_{L_3} = 0.03$	Normal
L_4	$\mu_{L_4} = 100$	$\sigma_{L_4} = 0.03$	Normal

Table 8. Random clearances of the combined trigonometric function mechanism

Variable	Clearance radius r_c (mm)	Distribution
$(X_1; Y_1)$	0.01	2D-uniform within a circle
$(X_2; Y_2)$	0.01	2D-uniform within a circle
$(X_3; Y_3)$	0.01	2D-uniform within a circle
$(X_4; Y_4)$	0.01	2D-uniform within a circle

The results are given in Table 9 and are plotted in Fig. 7. The sample size of MCS is 10^6, and the 95% confidence interval of the MCS solution is also provided in Table 9. The results show that proposed method is still accurate with the MCS solution as a reference. The error of the proposed method is smaller than 2.2% for time intervals from $\mu \in [55.68^{\circ}; 55.68^{\circ}]$ to $\mu \in [55.68^{\circ}; 155.68^{\circ}]$ (or time intervals from $\mu \in [0^{\circ}; 0^{\circ}]$ to $\mu \in [0^{\circ}; 100^{\circ}]$).

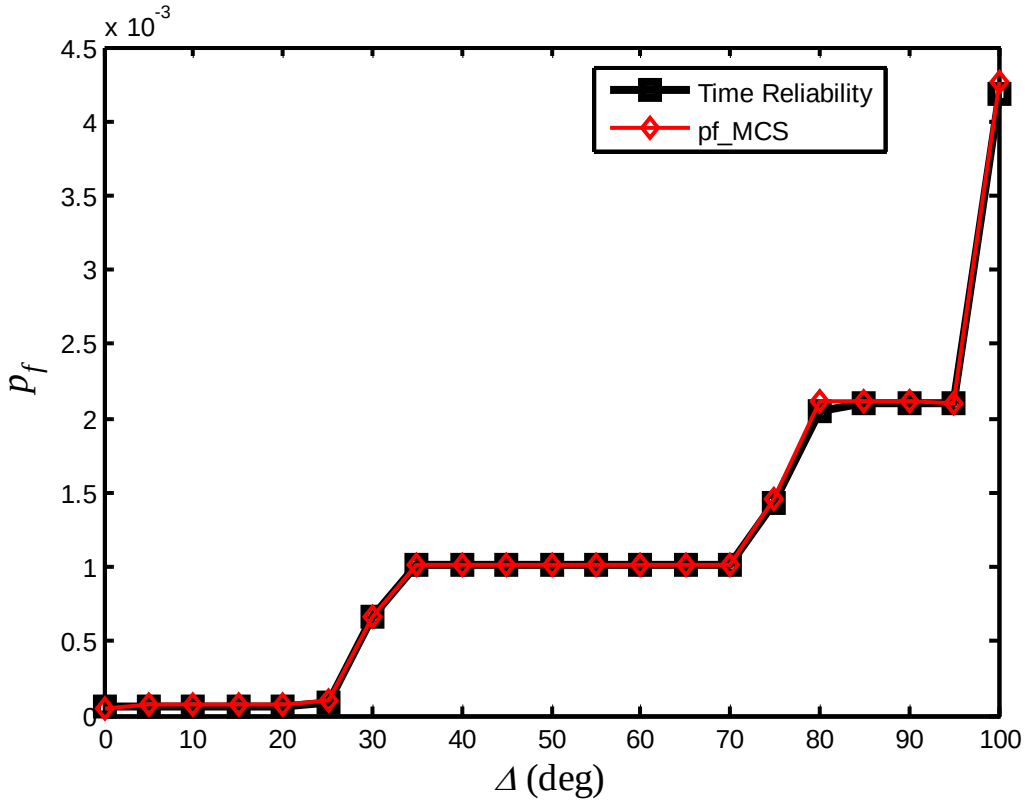

Figure 7 $p_f(\mu_0;\mu_e)$ of the combining trigonometric function mechanism

Table 9. $p_f(\mu_0;\mu_e)$ of the combining trigonometric function mechanism

$[\mu_0;\mu_e]$ $(^{\pm})$	Proposed method	MCS	95% MCS confidence interval	error (%)	Number of function evaluations	Computational time (seconds)	
						Proposed method	MCS
[55.68, 55.68]	6.44×10^{-5}	6.44×10^{-5}	$[5.94, 6.94]\times10^{-5}$	0.05	114	0.08	1.57
[55.68, 65.68]	6.44×10^{-5}	6.44×10^{-5}	$[5.94, 6.94]\times10^{-5}$	0.05	234	0.09	179
[55.68, 75.68]	6.44×10^{-5}	6.44×10^{-5}	$[5.94, 6.94]\times10^{-5}$	0.07	234	0.06	178
[55.68, 85.68]	6.70×10^{-4}	6.69×10^{-4}	$[6.53, 6.85]\times10^{-4}$	0.23	234	0.07	186
[55.68, 95.68]	1.01×10^{-3}	1.01×10^{-3}	$[0.95, 1.07]\times10^{-3}$	0.50	350	0.10	185
[55.68, 105.68]	1.01×10^{-3}	1.01×10^{-3}	$[0.95, 1.07]\times10^{-3}$	0.60	350	0.11	187
[55.68, 115.68]	1.01×10^{-3}	1.01×10^{-3}	$[0.95, 1.07]\times10^{-3}$	0.40	350	0.14	188
[55.68, 125.68]	1.01×10^{-3}	1.01×10^{-3}	$[0.95, 1.07]\times10^{-3}$	0.40	350	0.11	186
[55.68, 135.68]	2.07×10^{-3}	2.11×10^{-3}	$[2.02, 2.20]\times10^{-3}$	1.89	466	0.15	186
[55.68, 145.68]	2.10×10^{-3}	2.11×10^{-3}	$[2.02, 2.20]\times10^{-3}$	0.50	466	0.14	190
[55.68, 155.68]	4.17×10^{-3}	4.26×10^{-3}	$[4.14, 4.39]\times10^{-3}$	2.11	466	0.14	199

5. CONCLUSIONS

Inherent uncertainty exists in clearances of mechanisms. This uncertainty directly affects the performance of mechanisms. Qualifying its effect is critical. In this work, we develop an effective reliability analysis method to predict the kinematic reliability of function generation mechanisms by considering the uncertainty existing in both dimension variables and joint clearances for a given period of time.

The assumptions of the method include that the dimension variables are independently and normally distributed and that the 2-D or 3-D coordinates of the centers of joint pins are uniformity distributed within their clearance circles. The computational challenges present in two aspects. First, the motion output is time dependent, and the failures at different time instants in the given period of time are dependent. Second, the coordinates of a joint pin are dependent and are constrained within a circle or sphere. We tackle the challenges by employing the hybrid dimension reduction method to approximate the motion output with respect to random variables and also by employing the envelope method to account for the time dependence of the failures.

The three numerical examples, involving the sine, inverse tangent, and combined trigonometric function generators, respectively, demonstrate that the proposed method are both efficient and accurate. The errors of the probabilities of failure for the three mechanisms are smaller than 2.2%, except for the inverse tangent function generator for only one time period of time where the error is 6.22%. The three examples also indicate high computational efficiency as the reliability analysis could be completed within less than one second.

When the standard deviations of dimension variables and the radii of the joint clearances are large, the error from the proposed method may be large. This situation, however, is relatively rare for function generation mechanisms. As the three examples indicate, the errors for certain periods of time are still relatively large, and our future work will be the accuracy improvement.

Appendix Envelope Method

We briefly review the envelope method, and more details can be found in [29]. According to Eq. (16),

$$L(U;\mu) = b_0(1_S;\mu) + b(1_S;\mu)\,\phi U \tag{37}$$

where $b_0(1_S;\mu) = a_0$, and $b(1_S;\mu) = [a_{m\pounds 1};1_{q\pounds 1}]\,\phi\frac{3}{4}$, where $a = (a_1;a_2;\phi\phi\phi;a_m)$ $\frac{3}{4} = (\frac{3}{4}_L;\frac{3}{4}_c)$, $\frac{3}{4}_L = (\frac{3}{4}_{L_1};\frac{3}{4}_{L_2};\phi\phi\phi;\frac{3}{4}_{L_m})$ and $\frac{3}{4}_c = (\frac{3}{4}_{c_1};\frac{3}{4}_{c_2};\phi\phi\phi;\frac{3}{4}_{c_q})$. The task now becomes to find the envelope functions $G^+(U)$ and $G^i(U)$ for $L(U;\mu) = "$ and $L(U;\mu) = i\ "$, respectively.

According to Eq. (28), $G^+(U) = 0$ is given by

$$\begin{array}{l} L(U;\mu) = b_0(1_S;\mu) + b(1_S;\mu)\,\phi U = " \\ L_U(U;\mu) = b_{0_U}(1_S;\mu) + b(1_S;\mu)\,\phi U = 0 \end{array} \tag{38}$$

From the first line of Eq. (38),

$$U = \frac{[" i\ b_0(1_S;\mu)]b(1_S;\mu)}{b(1_S;\mu)\,\phi b(1_S;\mu)} \tag{39}$$

Plugging it into the second line of Eq. (38) yields

$$b_{0_U}(1_S;\mu) + [" i\ b_0(1_S;\mu)]\frac{b_U(1_S;\mu)\,\phi b(1_S;\mu)}{b(1_S;\mu)\,\phi b(1_S;\mu)} = 0 \tag{40}$$

There may be multiple solutions for μ from the above equation. As indicated in Eq. (29), the motion error at μ should be positive. We then eliminate those solutions where the motion errors are negative. Let the remaining solutions be μ_i^+, where $i = 1, 2, \cdots, p_i^+$. The expansion points are then

$$U(\mu_i^+) = \frac{[\varepsilon - b_0(1-s;\mu_i^+)]b(1-s;\mu_i^+)}{b(1-s;\mu_i^+)\cdot b(1-s;\mu_i^+)} \tag{41}$$

The envelope function $G^+(U) = 0$ can now be approximated by hyper-planes $L(U(\mu_i^+);\mu_i^+) = \varepsilon$, where $i = 1, 2, \cdots, p_i^+$. With the same principle, the envelope function $G^j(U) = 0$ can be approximated by $L(U(\mu_i^j);\mu_i^j) = \varepsilon$, where $i = 1, 2, \cdots, p_i^j$. The expansion points μ_i^j are given by

$$U(\mu_i^j) = -\frac{[\varepsilon + b_0(1-s;\mu_i^j)]b(1-s;\mu_i^j)}{b(1-s;\mu_i^j)\cdot b(1-s;\mu_i^j)} \tag{42}$$

Hence the time-dependent reliability is calculated by

$$R(\mu_0;\mu_e) = \Pr\left[\bigcap_{i=1}^{p^+} L(U;\mu_i^+) < \varepsilon \bigcup_{j=1}^{p^j} L(U;\mu_j^j) > -\varepsilon\right] \tag{43}$$

Also considering the two end points μ_0 and μ_e of the time interval, the time-dependent reliability is then given by

$$R(\mu_0;\mu_f) = \Pr\left[\bigcap_{i=1}^{p} z(U;\mu_i) < \varepsilon\right] \tag{44}$$

where $z(U;\mu_i) = s(\mu_i)L(U;\mu_i)$, μ_i includes μ_i^+, μ_i^j, μ_0, and μ_e, and $p = p_i^+ + p_i^j + 2$.

In Eq. (43), $s(\mu_i)$ is a sign function and defined by

$$s(\mu_i) = \begin{cases} 1 & \text{if } \mu = \mu_i^+ \\ -1 & \text{if } \mu = \mu_i^j \\ 1 & \text{if } \mu = \mu_0 \text{ or } \mu_e; L(U;\mu) \geq 0 \\ -1 & \text{if } \mu = \mu_0 \text{ or } \mu_e; L(U;\mu) \leq 0 \end{cases} \tag{45}$$

From Eq. (37), the approximated motion error $L(U;\mu)$ is normally distributed, and $s(\mu)L(U;\mu)$ in Eq. (44) is also normally distributed. The reliability can therefore be estimated by a multivariate normal distribution function with mean μ_z and covariance Σ, or $\Phi_p(\cdot;\mu_z;\Sigma)$; μ_z and Σ are given in Eqs. (43) and (44), respectively. Then the interval reliability can be estimated as discussed in Sec. 3.3.

ACKNOWLEDGEMENTS

The first author would like to thank the support from the following sources: the National Natural Science Foundation of China under Grant (No. 51275425), the Science and Technology Department of Sichuan Province (No. 2009JY0138), the Chunhui Project of the Education Ministry of China (No. Z2011081), and the Key Laboratory of Manufacturing and Automation of Sichuan Province at Xihua University.

The second author would also like to acknowledge the support from the Intelligent Systems Center at the Missouri University of Science and Technology.

REFERENCES

[1] S. Erkaya, İ. Uzmay, Determining link parameters using genetic algorithm in mechanisms with joint clearance, Mechanism and Machine Theory, 44 (2009) 222-234.
[2] J. Zhu, K.-L. Ting, Uncertainty analysis of planar and spatial robots with joint clearances, Mechanism and Machine Theory, 35 (2000) 1239-1256.
[3] M.-J. Tsai, T.-H. Lai, Kinematic sensitivity analysis of linkage with joint clearance based on transmission quality, Mechanism and Machine Theory, 39 (2004) 1189-1206.
[4] M.-J. Tsai, T.-H. Lai, Accuracy analysis of a multi-loop linkage with joint clearances, Mechanism and Machine Theory, 43 (2008) 1141-1157.
[5] K.-L. Ting, J. Zhu, D. Watkins, The effects of joint clearance on position and orientation deviation of linkages and manipulators, Mechanism and Machine Theory, 35 (2000) 391-401.
[6] V. Parenti-Castelli, S. Venanzi, Clearance influence analysis on mechanisms, Mechanism and Machine Theory, 40 (2005) 1316-1329.

[7] P. Flores, J. Ambrósio, Revolute joints with clearance in multibody systems, Computers & Structures, 82 (2004) 1359-1369.
[8] S. Erkaya, Trajectory optimization of a walking mechanism having revolute joints with clearance using ANFIS approach, Nonlinear Dynamics, 71 (2013) 75-91.
[9] S. Erkaya, Investigation of joint clearance effects on welding robot manipulators, Robotics And Computer-Integrated Manufacturing, 28 (2012) 449-457.
[10] P. Flores, Ambrosio, J., Claro, H.C.P., Lankarani, H.M., Koshy, C.S., A study on dynamics of mechanical systems including joints with clearance and lubrication, Mechanism and Machine Theory, 41 (2006) 247-261.
[11] P. Flores, Modeling and simulation of wear in revolute clearance joints in multibody systems, Mechanism and Machine Theory, 44 (2009) 1211-1222.
[12] Q. Tian, Liu, C., Machado, M., Flores, P., A new model for dry and lubricated cylindrical joints with clearance in spatial flexible multibody systems, Nonlinear Dynamics, 64 (2011) 25-47.
[13] P. Flores, Koshy, C.S., Lankarani, N.M., Ambrosio, J., Claro, J.C.P., Numerical and experimental investigation on multibody systems with revolute clearance joints, Nonlinear Dynamics, 65 (2011) 383-398.
[14] P. Flores, J. Ambrósio, On the contact detection for contact-impact analysis in multibody systems, Multibody System Dynamics, 24 (2010) 103-122.
[15] S.M. Varedi, H.M. Daniali, M. Dardel, A. Fathi, Optimal dynamic design of a planar slider-crank mechanism with a joint clearance, Mechanism and Machine Theory, 86 (2015) 191-200.
[16] Z. Zhang, L. Xu, P. Flores, H.M. Lankarani, A kriging model for the dynamics of mechanical systems with revolute joint clearances, Journal of Computational and Nonlinear Dynamics, 9 (2014) 031013.
[17] X. Zhang, X. Zhang, Z. Chen, Dynamic analysis of a 3-RRR parallel mechanism with multiple clearance joints, Mechanism and Machine Theory, 78 (2014) 105-115.
[18] S. Erkaya, İ. Uzmay, Optimization of transmission angle for slider-crank mechanism with joint clearances, Structural And Multidisciplinary Optimization, 37 (2009) 493-508.
[19] S. Erkaya, İ. Uzmay, A neural-genetic (NN-GA) approach for optimising mechanisms having joints with clearance, Multibody System Dynamics, 20 (2008) 69-83.
[20] C. Innocenti, Kinematic clearance sensitivity analysis of spatial structures with revolute joints, Journal of Mechanical Design, 124 (2002) 52-57.
[21] A. H. Chebbi, Z. Affi, L. Romdhane, Prediction of the pose errors produced by joints clearance for a 3-UPU parallel robot, Mechanism and Machine Theory, 44 (2009) 1768-1783.
[22] A. Frisoli, M. Solazzi, D. Pellegrinetti, M. Bergamasco, A new screw theory method for the estimation of position accuracy in spatial parallel manipulators with revolute joint clearances, Mechanism and Machine Theory, 46 (2011) 1929-1949.
[23] J. Meng, D. Zhang, Z. Li, Accuracy analysis of parallel manipulators with joint clearance, Journal of Mechanical Design, 131 (2009) 011013.
[24] W. Wu, S.S. Rao, Uncertainty analysis and allocation of joint tolerances in robot manipulators based on interval analysis, Reliability Engineering and System Safety, 92 (2007) 54-64.

[25] G. Chen, H. Wang, Z. Lin, A unified approach to the accuracy analysis of planar parallel manipulators both with input uncertainties and joint clearance, Mechanism and Machine Theory, 64 (2013) 1-17.
[26] J. Wang, J. Zhang, X. Du, Hybrid dimension reduction for mechanism reliability analysis with random joint clearances, Mechanism and Machine Theory, 46 (2011) 1396-1410.
[27] S.G. Dhande, J. Chakraborty, Mechanical error analysis of spatial linkages, Journal of Mechanical Design 100 (1977) 732-738.
[28] W. Xu, Q. Zhang, Probabilistic analysis and Monte Carlo simulation of the kinematic error in a spatial linkage, Mechanism and Machine Theory, 24 (1989) 19-27.
[29] J. Chakraborty, Synthesis of mechanical error in linkages, Mechanism and Machine Theory, 10 (1975) 155-165.
[30] A.K. Mallik, S.G. Dhande, Analysis and synthesis of mechanical error in path-generating linkages using a stochastic approach, Mechanism and Machine Theory, 22 (1987) 115-123.
[31] J.H. Choi, S.J. Lee, D.H. Choic, Stochastic linkage modeling for mechanical error analysis of planar mechanisms, Mechanics of Structures and Machines, 26 (1998) 257-276.
[32] P.K. Bhatti, Probabilistic modeling and optimal design of robotic manipulators, in, Purdue University, West Lafayette,Indiana, 1989.
[33] X. Du, P.K. Venigella, D. Liu, Robust mechanism synthesis with random and interval variables, Mechanism and Machine Theory, 44 (2009) 1321-1337.
[34] Z. Shi, X. Yang, W. Yang, Robust synthesis of path generating linkages, Mechanism and Machine Theory, 40 (2005) 45-54.
[35] M.D. Pandey, X. Zhang, System reliability analysis of the robotic manipulator with random joint clearances, Mechanism and Machine Theory, 58 (2012) 137-152.
[36] J. Kim, W. Song, B. Kang, Stochastic approach to kinematic reliability of open-loop mechanism with dimensional tolerance, Applied Mathematical Modelling, 34 (2010) 1225-1237.
[37] J. Zhang, J. Wang, X. Du, Time-dependent probabilistic synthesis for function generator mechanisms, Mechanism and Machine Theory, 46 (2011) 1236-1250.
[38] J. zhang, X. Du, Time-dependent reliability analysis for function generator mechanisms, Journal of Mechanical Design, 133 (2010) 031005.
[39] X. Du, Time-dependent mechanism reliability analysis with envelope functions and first-order approximation, Journal of Mechanical Design, 136 (2014) 081010.
[40] E. A. DeVuyst, P. V. Preckel, Gaussian cubature: A practitioner's guide, Mathematical and Computer Modelling, 45 (2007) 787-794.
[41] M. Abramowitz, I. Stegun, Handbook of mathematical functions with formulas, graphs, and mathematical tables, Dover publications, 1964.